

The parallel-antiparallel signal difference in double-wave-vector diffusion-weighted MR at short mixing times: A phase evolution perspective

Jürgen Finsterbusch*

Department of Systems Neuroscience, University Medical Center Hamburg–Eppendorf, Hamburg, Germany
Neuroimage Nord, University Medical Centers Hamburg–Kiel–Lübeck, Germany

ARTICLE INFO

Article history:

Received 5 August 2010

Revised 20 October 2010

Available online 25 October 2010

Keywords:

Double-wave-vector diffusion weighting

Multiple-wave-vector diffusion weighting

Phase evolution

Phase gymnastics

Cell size

Pore size

ABSTRACT

Experiments with two diffusion weightings applied in direct succession in a single acquisition, so-called double- or two-wave-vector diffusion-weighting (DWV) experiments at short mixing times, have been shown to be a promising tool to estimate cell or compartment sizes, e.g. in living tissue. The basic theory for such experiments predicts that the signal decays for parallel and antiparallel wave vector orientations differ by a factor of three for small wave vectors. This seems to be surprising because in standard, single-wave-vector experiments the polarity of the diffusion weighting has no influence on the signal attenuation. Thus, the question how this difference can be understood more pictorially is often raised. In this rather educational manuscript, the phase evolution during a DWV experiment for simple geometries, e.g. diffusion between parallel, impermeable planes oriented perpendicular to the wave vectors, is considered step-by-step and demonstrates how the signal difference develops. Considering the populations of the phase distributions obtained, the factor of three between the signal decays which is predicted by the theory can be reproduced. Furthermore, the intermediate signal decay for orthogonal wave vector orientations can be derived when investigating diffusion in a box. Thus, the presented “phase gymnastics” approach may help to understand the signal modulation observed in DWV experiments at short mixing times.

© 2010 Elsevier Inc. All rights reserved.

1. Motivation

Double-wave-vector diffusion-weighting (DWV) experiments [1–4] with short mixing times involve two diffusion-weighting periods applied in direct succession in a single acquisition (Fig. 1a). In a first theoretical approach [3], it has been shown that the signal amplitude of such experiments depends on the angle between the two wave vectors θ , for small wave vectors with $\cos\theta$, but only if the diffusion is restricted (see Appendix A). The amplitude of this restriction-specific modulation is proportional to the so-called mean-squared radius of gyration of the pores which increases with the pore size. Thus, such experiments have been shown to be a promising tool to investigate a sample’s microstructure [5–8] and are of particular interest for the characterization of tissue *in vivo* [9,10].

The simplest and most reliable way to observe this restriction effect and estimate pore or cell sizes is to apply two experiments, with parallel and with antiparallel wave vector orientations, i.e. to sample the maximum and minimum of the signal modulation. Thereby,

the signal decay present for the parallel wave vector orientation is expected to be three times that of the antiparallel orientation according to the theory (see Appendix A) [3]. This signal difference is often considered to be strange because both experiments differ only by the polarity of one of the wave vectors and such an inversion has no effect on the diffusion-weighted signal in simple single-wave-vector experiments with one diffusion-weighting period. Furthermore, the b values of the parallel and antiparallel orientation are equal for non-overlapping diffusion-weighting periods (Fig. 1a) which means that no signal difference shows up for freely diffusing spins. Thus, although the mathematical equations are not called into question, there seems to be the need for a more vivid point-of-view of the origin of this signal difference.

The present manuscript is an attempt to present such a perspective by considering the step-by-step phase evolution (“phase gymnastics”) in simple geometries during a short-mixing-time DWV experiment. Thus, it will neither report novel scientific results nor predict new effects but aims to provide a better understanding of the principles underlying the described signal modulation.

2. Phase evolution

In accordance with the basic theory [3] (see Appendix), the phase evolution will be considered for restricted geometries under

* Address: Institut für Systemische Neurowissenschaften, Geb. W34, Universitätsklinikum Hamburg-Eppendorf, 20246 Hamburg, Germany. Fax: +49 40 7410 59955.

E-mail address: j.fensterbusch@uke.uni-hamburg.de

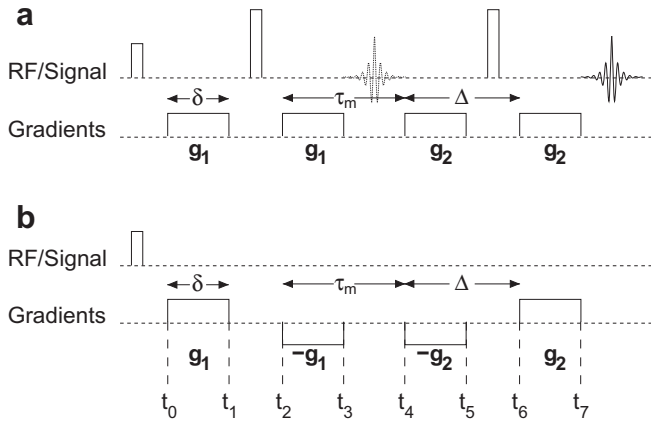


Fig. 1. Basic pulse sequences for the double-wave-vector (DWV) experiment. The variant without refocussing RF pulses shown in (b) was used for the considerations of the phase evolution. Note that the diffusion-weighting scheme in (a) and (b) corresponds to a parallel orientation of the two wave vectors.

the assumption of short gradient pulse durations δ , i.e. an instantaneous decoding of the spins' phases, a long diffusion time that ensures a complete mixing of spins from any position, and a short mixing time τ_m , however, without an overlap of the two diffusion-weighting periods, i.e. with $\tau_m = \delta$ (Fig. 1a).

For clarity, the pulse sequence of Fig. 1b will be used, where no refocussing RF pulses are applied. Furthermore, only parallel, antiparallel, and orthogonal wave vectors are considered. Note that “parallel” as defined in [3] and used herein, means that the rephasing gradient of the first wave vector and the dephasing gradient of the second wave vector have the same polarity as shown in Fig. 1a and b.

2.1. Diffusion between parallel planes

As a simple example, diffusion of spins between parallel, impermeable planes oriented perpendicular to the parallel or antiparallel wave vectors, is investigated for a constant spin density (see Fig. 2). For simplicity, it is assumed that the planes are centered around the isocenter, i.e. spins in the middle between the two planes are

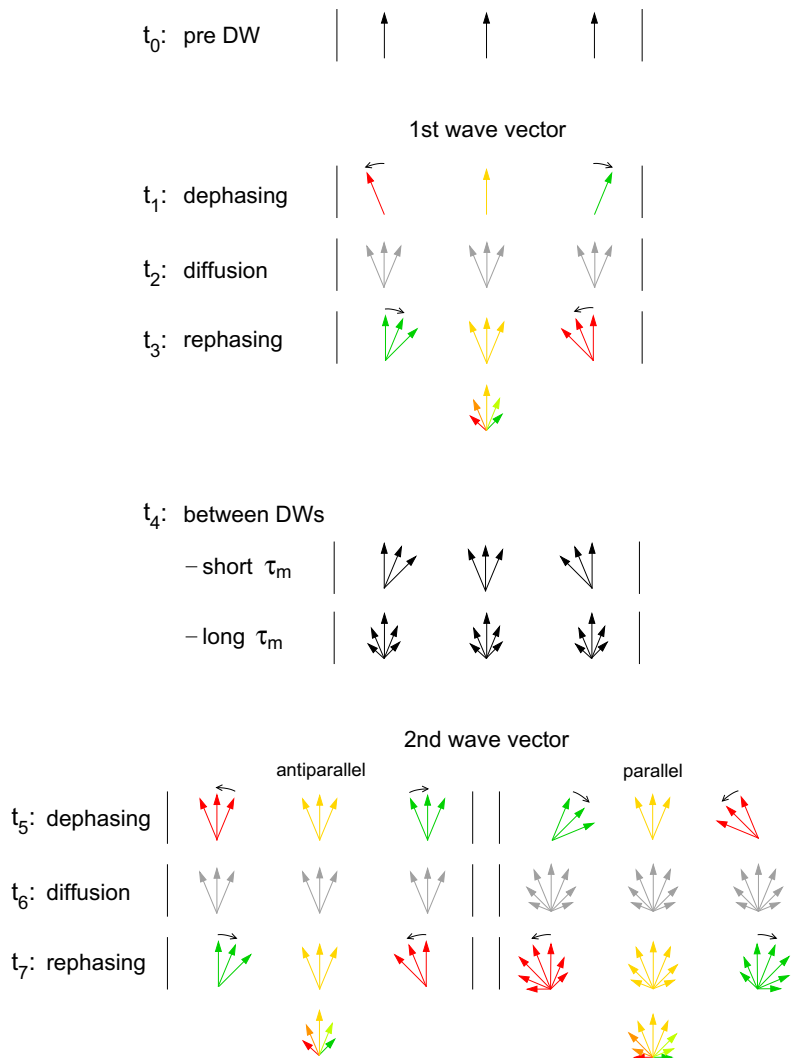


Fig. 2. Schematic phase diagrams for three different positions between the two planes (outermost left, center, and outermost right) at the different times of the DWV experiment indicated in Fig. 1b for parallel wave vector orientations. The time points t_5 – t_7 were obtained for a short mixing time. At the final time t_7 , the phases cover a larger range with a broader distribution for parallel wave vectors, which yields a higher signal decay. Note that the arrow lengths were chosen to qualitatively reflect the relative phase populations which are considered in details in Fig. 3. For details see text.

not affected (yellow) by the diffusion gradient pulses while those touching the planes yield a maximum phase tilt of α in opposite directions, either positive (green; small, curved arrow pointing right) or negative (red; small, curved arrow pointing left), respectively.

Fig. 2 demonstrates the phase evolution during the DWV experiment shown in Fig. 1b for parallel and antiparallel wave vector orientations. Note that the relative arrow lengths in each “bouquet” of arrows qualitatively reflect the relative population of the corresponding phase which will be considered in more detail below.

Prior to the first diffusion-weighting gradient pulse (t_0), the spins are in phase yielding the maximum magnetization. The first, dephasing gradient pulse changes the phase of the spins, at the outermost positions by $\pm\alpha$ (t_1). During the diffusion time which was assumed to be long, the spins from all positions have time to diffuse to anywhere between the two planes. This implies that at the end of the diffusion time (t_2) (i) the same phase distribution is found at any position between the planes and (ii) it represents a mixture of all spin phases present prior to the diffusion time, i.e. a uniform distribution between $\pm\alpha$. The second, rephasing gradient (t_3) tilts these distributions by up to $\mp\alpha$, i.e. in a direction opposite to the first, dephasing gradient pulse. Thus, the spins’ phases between the planes are distributed over an angular range of 4α . It is obvious that this phase dispersion yields an overall signal that is reduced compared to the initial magnetization which reflects the diffusion-induced signal attenuation of the (single-wave-vector) experiment considered so far. For a short-mixing-time experiment, the phases will not change during the mixing time (t_4).

To consider the effect of the second wave vector the two cases of a parallel (right panel) and an antiparallel wave vector orientation (left panel) are distinguished. For the antiparallel orientation, the third, dephasing gradient has an inverted polarity compared to the second, rephasing one, i.e. the phase tilt introduced by that gradient pulse is compensated, because short gradient pulses were assumed, immediately and completely. This also means that the phase distribution after the third gradient pulse (t_5) is identical to that prior to the second: a spatially uniform distribution covering the range between $-\alpha$ and $+\alpha$ at any position. The second diffusion time then has no additional effect because identical distributions are mixed up (t_6). The final, rephasing gradient then tilts the phases again by $\pm\alpha$ and exactly reproduces the phase distribution observed after the first rephasing gradient (t_7).

The fact that the second diffusion weighting does not provide any additional effect, is obvious if the assumptions are recalled. Effectively, the second and third gradient cancel each other immediately ($\delta, \tau_m \rightarrow 0$), which means that the two-wave-vector experiment with antiparallel orientations is identical to a single-wave-vector experiment with the doubled diffusion time. However, as the diffusion was assumed to be long ($\Delta \rightarrow \infty$), a further prolongation has no additional effect.

This is different for the parallel wave vector orientation, where the third, dephasing gradient pulse amplifies the phase tilt introduced by the preceding gradient (t_5) which is the crucial difference between the two orientations. Thus, the angular range covered by the phases is further increased by 2α yielding 6α in total if all positions are taken into account. During the second diffusion time, the spins mixup again completely and at the end of the diffusion time (t_6) the phase distribution is identical at all positions spanning an angle of 6α . The final, rephasing gradient adds another tilt by $\pm\alpha$ (t_7) distributing the phases over a total range of 8α .

Thus, the phases cover a larger range than for the antiparallel orientation (4α) which explains the higher signal decay for the parallel orientation. For a more detailed exploitation, the populations of the different phase states need to be considered which is performed in the next section.

2.2. Phase distributions

In Fig. 3, the phase distributions present at the different times considered in Fig. 2 are sketched. Thereby, two distributions are distinguished. First, shown in the left panels, the local phase distribution which describes the phases relative to the local mean (or center) phase at each position. This distribution is the same for all different spatial positions within the sample at any time: for each time point, the arrow “bouquets” for the three positions between the planes shown in Fig. 2 differ only by a rotation of the whole “bouquets”. Second, presented in the middle panels, the distribution of the center phases for the different positions between the planes, i.e. the angle the “bouquets” are rotated by, at the different positions. Because the local distribution is present at each center position, the total phase distribution within the sample (right panels) is simply the convolution of these two distributions.

Since the effects of the different gradient pulses and diffusion times on the phases are shown in Fig. 2 and have been described above in detail, only a short repetition with respect to the specific phase distribution is given here. Prior to the first diffusion gradient (t_0), all phases are identical, i.e. the local as well as the mean phase distribution represent δ functions. The first, dephasing gradient, causes a distribution of the center phase between $-\alpha$ and α while the local distribution is still a δ function (t_1): at each position only a unique phase is present. After the diffusion time (t_2), the total phase distribution present prior to the diffusion time is found at any position, i.e. the local phase distribution is identical to the total prior to the diffusion time, while the center phase distribution is again equal to a δ function (note that these changes do not alter the total phase distribution as expected). With the second, rephasing gradient (t_3), the center phase again is uniformly distributed within $\pm\alpha$ which yields a triangular total phase distribution between $\pm 2\alpha$.

For the antiparallel wave vector orientation, the third, dephasing gradient (t_5) changes the center phase distribution back to a δ function while the final, rephasing gradient (t_7) restores the uniform distribution between $\pm\alpha$, i.e. the triangular total phase distribution between $\pm 2\alpha$ as for t_3 .

For the parallel orientation, the third, dephasing gradient (t_5) spreads the center phases over a range of $\pm 2\alpha$ which is the important contrast to the δ function for the antiparallel case. It changes the total phase distribution to a trapezoidal shape covering $\pm 3\alpha$. During the diffusion time, the local phase distribution is replaced by the trapezoidal total distribution while the center phase distribution collapses to a δ function (t_6). The last, rephasing gradient (t_7) again causes a uniform center phase distribution between $\pm\alpha$. Thus, a bell-shaped, piecewise quadratic total phase distribution is obtained which is broader than the corresponding distribution for the antiparallel orientation (gray line).

The effective signal amplitudes resulting from the two total phase distributions observed after the second wave vector, the triangular for the antiparallel and the piecewise quadratic for the parallel wave vector orientation, are considered in Appendix B for small wave vectors. A factor of three is easily obtained for the relative signal decays which is consistent with the theory (see Appendix A). But it should be emphasized that the phase distributions were derived exactly, i.e. they are valid for any wave vector amplitude. Thus, this model could also provide a simple approach to compute higher order effects within the short-pulse approximation.

2.3. Long mixing time and finite timing parameters

The short mixing time between the two wave vectors is crucial to observe the difference between the two wave vector orientations. For a long mixing time (see Fig. 2), all spins will be redistributed

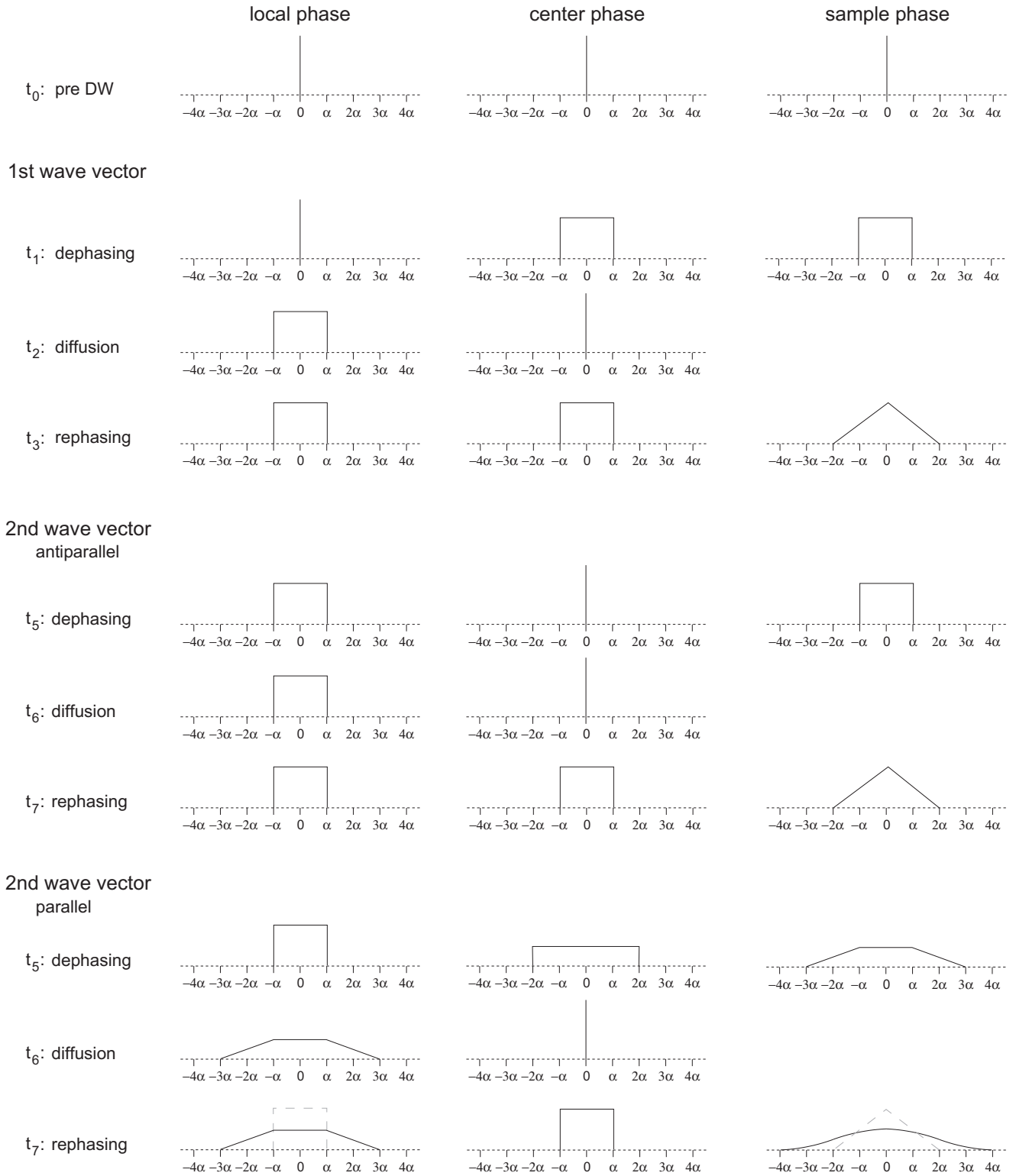


Fig. 3. Local phase distribution (left), i.e. the phase distribution at a single position between the two planes relative to its mean, center phase distribution (middle), i.e. the distribution of the mean phase for the different positions, and the total phase distribution in the sample (right) for the different times of the DWV experiment indicated in Fig. 1b. The local phase distribution is identical for all spatial positions for each time point shown. Thus, the sample's phase distribution is the convolution of the local and the center phase distribution. At the final time t_7 , the distribution in the sample (lower right) is much broader for parallel wave vector orientations (solid) than that of the antiparallel orientation (dashed line). For details see text.

between the planes within the mixing time. This yields identical distributions spanning an angle of 4α at any position (see Fig. 2). In other words, the asymmetry between left and right positions is lost.

For such a mirror-symmetric phase distribution, the polarity of the second wave vector does not matter and identical signals are obtained for both orientations.

Similarly, finite gradient pulse durations and diffusion times reduce the signal difference. For short diffusion times, the mixup will be incomplete and the phase distributions at each position will still reflect the phase tilt induced by the dephasing gradient at that position. Thus, the rephasing gradient will compensate for some of the phase tilt which reduces the angular range covered and, thus, the signal difference. This also holds for long gradient pulses. Because they do not perform an instantaneous phase tilt, the spins can diffuse during the encoding. The accumulated phase tilt then represents the averaged phase tilt along their path. Thus, extreme phases like $\pm\alpha$ are lost and the total angular phase range covered is reduced.

2.4. Diffusion in a box

Now the diffusion of spins in a quadratic box will be considered (Fig. 4a). It is assumed to be in the isocenter, and the wave vectors are supposed to be oriented perpendicular to the restricting walls with the first wave vector along the left–right direction without loss of generality (w.l.o.g.). The second wave vector is assumed to be in a parallel, antiparallel, or orthogonal orientation, the latter, w.l.o.g., in up–down direction. As for the parallel planes, the spins in the center of the box are unaffected by the gradient pulses for both, left–right and up–down wave vector directions. The phases of the spins in the left and right column are tilted in opposite directions for wave vectors along the left–right directions, the phases of the spins in the upper and lower row accordingly for a wave vector along the up–down direction.

For the phase evolution during a diffusion period, only the position coordinate along the direction of the corresponding wave vector is relevant. This means that different coordinates in a perpendicular direction need not to be distinguished but can be considered together. For instance, for the first wave vector (left–right), the spins within each of the individual columns (left, middle, right) will be affected equally and can be merged to a single arrow “bouquet”. Because prior to the wave vector, the phases are identical, the corresponding “bouquets” contain only a single phase (Fig. 4a).

The phase evolutions and distributions for the first wave vector and even for two wave vectors with parallel or antiparallel orientation are identical to those presented in Figs. 2 and 3 for the parallel planes. Of course, the diffusion in up–down direction differs for the two geometries but this displacement is not encoded by gradient pulses as both wave vectors were assumed to be oriented along the left–right direction. However, this is different for the orthogonal direction as will be seen below.

Note that these arguments analogously apply for a cubic box (Fig. 4a). In this case, any diffusion motion in the third direction (front–back) does not alter the phase evolution, i.e. the phase evolutions and distributions for the combinations considered above (parallel, antiparallel) remain valid as well.

2.5. Orthogonal wave vector orientation

For the boxes, an orthogonal wave vector orientation can be considered because the diffusion is restricted in two orthogonal directions. The first wave vector will again be assumed in the left–right direction which yields phase evolutions and distributions identical to that of Figs. 2 and 3 for t_0 – t_4 (short τ_m). The second wave vector is assumed to be along the up–down direction. As noted above, it then is sufficient to distinguish only upper, middle, and lower positions during this wave vector’s diffusion period. However, the different phases present in each “row” or horizontal “plane” prior to the second wave vector (t_4 for short τ_m) must be considered and combined to a “bouquet” of the phases at the corresponding left, middle, and right positions as shown in Fig. 4b. These “bouquets” are identical for the upper, middle, and lower

row or plane because the phases were caused by the first wave vector which was applied in left–right direction. These “bouquets” span an angle of 4α and represent the initial configuration for the phase evolution during the second (orthogonal) wave vector which is presented in Fig. 4c.

For the time point t_4 , i.e. after τ_m which is assumed to be short, the different vertical positions share the same phase distribution. Again the third, dephasing gradient pulse introduces a tilt of $\pm\alpha$, now for the upper and lower positions, respectively (t_5). During the diffusion time, the phases are again completely mixed yielding identical distributions covering 6α for all positions (t_6). The final, rephasing gradient adds another α tilt (t_7) which yields a total distribution of 8α .

This range is significantly larger than for the antiparallel orientation but is identical for the parallel case. However, the populations are different compared to the parallel orientation: less spins have phases with a large tilt angles of $\pm 3\alpha$ or more while more spins have smaller tilts of $\pm\alpha$ or below. Thus, the signal amplitude for the orthogonal orientation is lower than for the antiparallel orientation but larger than for the parallel case. This can be seen more clearly by considering the explicit populations of the different phase states.

The populations are shown in Fig. 4c. As can be seen in Fig. 4b, the local phase distribution in all three rows or planes considered is identical to the total phase distribution in the sample after the first wave vector, i.e. it is the triangular distribution of t_3 in Fig. 3. The third, dephasing gradient pulse (t_5) causes a distribution of the central phase yielding a piecewise quadratic total phase distributions between -3α and $+3\alpha$. This distribution is the local phase distribution after the diffusion time while the center phase distribution again has collapsed to a δ function. The final, rephasing gradient converts the central phase distribution to a rectangular distribution. Thus, the total phase distribution now is the convolution of a piecewise quadratic distribution with a rectangular function which yields a piecewise cubic distribution. Although it is also based on the range between $\pm 4\alpha$, it is “sharper” than the quadratic distribution of the parallel orientations (solid gray line) because the areas, the number of spins, are equal. Thus, the piecewise cubic distribution has more spins with phases within $\pm\alpha$ and less spins with phases beyond $\pm 2\alpha$. Thus, the corresponding signal decay is lower than for parallel wave vectors but exceeds that of the antiparallel orientations which is restricted $\pm 2\alpha$ (dashed gray line). A detailed calculation analogous to that performed in Appendix B is straightforward and yields a decay of $2\alpha^2/3$ which, in consistency with the theory, is the average of the decays for parallel and antiparallel orientations.

3. Summary

The phase evolution for a DWV experiment at short mixing times was investigated for two simple example geometries, e.g., diffusion between parallel planes oriented perpendicular to the wave vectors. It can explain the signal difference between parallel and antiparallel wave vector orientations more comprehensively and vividly. Taking the populations of the phase states into account, the factor of three for the signal decays expected from the theory is reproduced. Analogously, the signal decay for an orthogonal wave vector orientation can be obtained for spins diffusing in a box. It yields the average of the parallel and antiparallel decays which is also consistent with the theory.

Thus, the presented phase evolution approach reproduces the crucial property of a DWV experiment at short mixing time, the three-fold higher signal decay for parallel compared to antiparallel wave vector orientations, in simple example systems from a more pictorial point-of-view and may help to facilitate the understanding of the underlying effect.

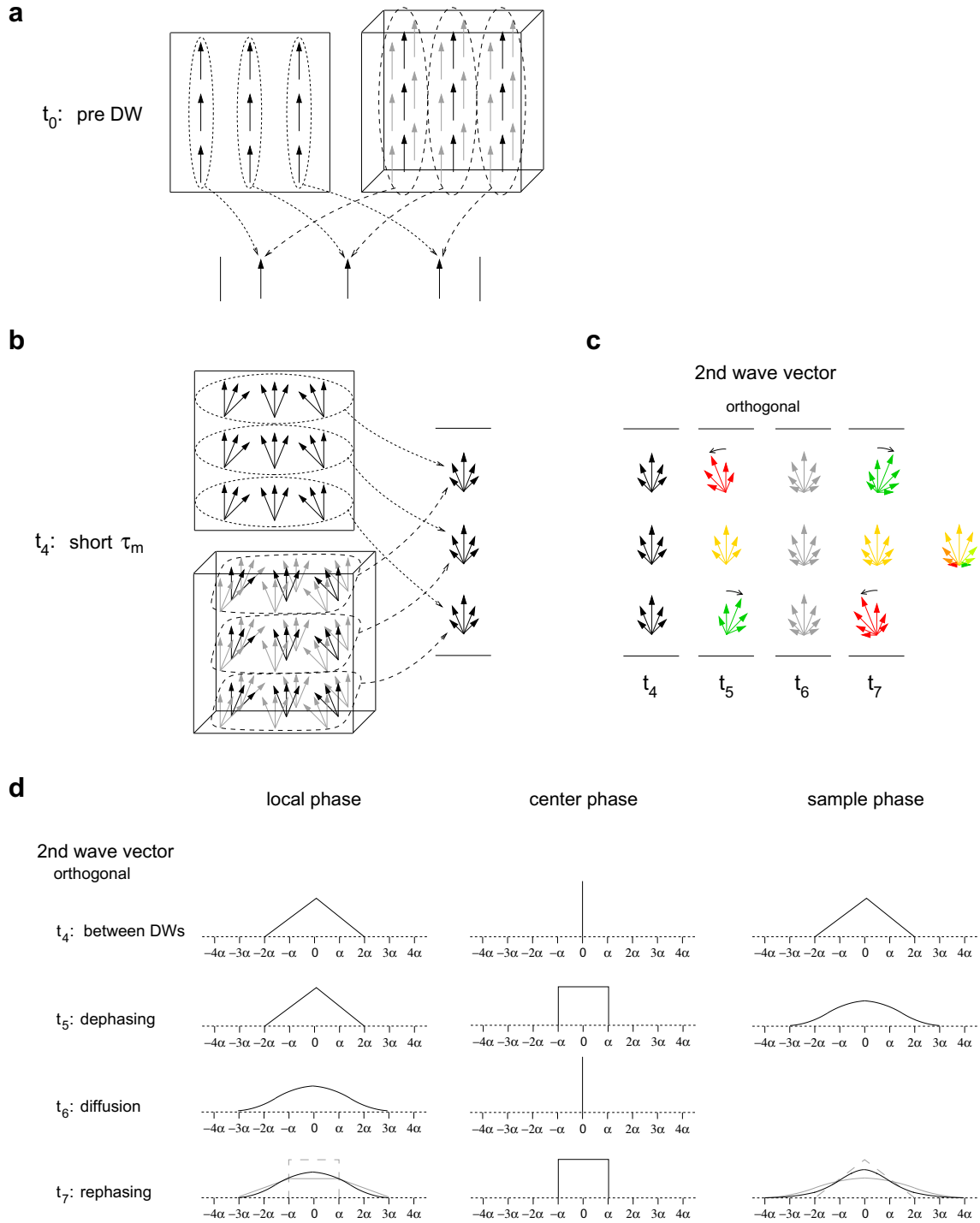


Fig. 4. (a) Basic approach to consider spins diffusing in a quadratic or cubic box with the wave vector oriented along the left–right direction. Because only the position coordinate along the wave vector direction is relevant, all spins sharing the same coordinate can be considered together. (b) Phase distribution in a quadratic and cubic box after the first diffusion-weighting period with the wave vector along the left–right direction (see Fig. 2). To consider the phase evolution during the second diffusion-weighting, where the wave vector is applied in up–down direction, the phases in a row or horizontal plane can be merged to a single “bouquet” of arrows as their further evolution will be identical. In the cubic box of (a) and (b), the frontal and backwards phases are shown in gray for clarity. (c) Schematic phase diagrams for the three different rows or planes (uppermost, middle, and lowermost) in a box as shown in (b) at the different times during the second diffusion-weighting period of a short-mixing-time DWV experiment (see Fig. 1b). Note that the arrow lengths were chosen to qualitatively reflect the relative phase populations which are considered in details in (d). (d) Local (left), center (middle), and total (right) phase distributions during the second diffusion-weighting period for orthogonal wave vectors. After the last rephasing gradient pulse (t_7), the total phase distribution is narrower (sharper) than for a parallel orientation (solid gray line) but broader than for an antiparallel orientation (dashed), i.e. an intermediate signal is obtained. For details see text.

Acknowledgment

Parts of this work were supported by Bundesministerium für Bildung und Forschung (Neuroimage Nord).

Appendix A. Theory

Under the assumption of (i) short gradient pulse durations δ , i.e. $\delta \rightarrow 0$ for a constant wave vector amplitude q , (ii) a short mixing time $\tau_m \rightarrow 0$ (cf. Fig. 1), (iii) long diffusion times Δ , i.e. $\Delta \rightarrow \infty$, (iv) fully restricted diffusion, and (v) an isotropic orientation distribution of identical pores, the MR signal of a DWV experiment according to Fig. 1a, expanded to second order, has been shown to obey [3]

$$M(\mathbf{q}_1, \mathbf{q}_2) \propto 1 - \frac{1}{3} q^2 \langle R^2 \rangle (2 + \cos \theta) \quad (\text{A.1})$$

where \mathbf{q}_1 and \mathbf{q}_2 are the two wave vectors with $\mathbf{q}_i = \gamma \delta \mathbf{G}_i$ ($q_1 = q_2 = q$, γ : gyromagnetic ratio, \mathbf{G} : gradient amplitude), θ is the angle between the two wave vectors, i.e. $\cos \theta = \mathbf{q}_1 \cdot \mathbf{q}_2 / q_1 q_2$, and $\langle R^2 \rangle$ is the mean-squared radius of gyration

$$\langle R^2 \rangle = \int_{\text{pore}} r^2 \rho(\mathbf{r}) d\mathbf{r} \quad (\text{A.2})$$

with the spin density $\rho(\mathbf{r})$.

Equation (A.1) is an approximation for small wave vectors. It implies that the signal decay for a parallel wave vector orientation ($\theta = 0^\circ$) is three times that for an antiparallel orientation ($\theta = 180^\circ$). Furthermore, the signal for orthogonal wave vector orientations ($\theta = 90^\circ$) is expected to be the average of the signal for parallel and antiparallel orientations.

Appendix B. Signal calculations

For arbitrary experiments, the signal within a given volume can be calculated by considering the spin density and the phase $\varphi(\mathbf{r})$ according to

$$M = \int_{\text{volume}} \rho(\mathbf{r}) e^{i\varphi(\mathbf{r})} d\mathbf{r} \quad (\text{A.3})$$

which is valid for any q . If the phases φ are limited to a small range of values, for instance because only a small wave vector q was used in diffusion-weighted experiments ($\varphi \propto q$), the phase factor can be expanded which, performed up to second order (Gaussian phase approximation), yields

$$M = \int_{\text{volume}} \rho(\mathbf{r}) \left(1 + i\varphi(\mathbf{r}) - \frac{1}{2} \varphi^2(\mathbf{r}) \right) d\mathbf{r} \quad (\text{A.4})$$

which can be converted to an integration over φ

$$M = \int_{-\pi}^{\pi} \rho(\varphi) \left(1 + i\varphi - \frac{1}{2} \varphi^2 \right) d\varphi \quad (\text{A.5})$$

where $\rho(\varphi)$ denotes the population density of the phase φ , i.e. the phase distribution function considered in the manuscript. Defining the mean phase as zero, i.e. $\int \rho(\mathbf{r}) \varphi(\mathbf{r}) d\mathbf{r} = 0$, Eq. (A.5) reduces to

$$M = \int_{-\pi}^{\pi} \rho(\varphi) d\varphi - \frac{1}{2} \int_{-\pi}^{\pi} \rho(\varphi) \varphi^2 d\varphi = 1 - \frac{1}{2} \int_{-\pi}^{\pi} \rho(\varphi) \varphi^2 d\varphi \quad (\text{A.6})$$

For the triangular phase distribution of the antiparallel wave vector orientation, the signal calculation is straightforward:

$$\begin{aligned} M_{\text{anti}} &= 1 - \frac{1}{2} \int_{-2\alpha}^{+2\alpha} \rho_{\text{anti}}(\varphi) \varphi^2 d\varphi = 1 - \int_0^{2\alpha} \rho_{\text{anti}}(\varphi) \varphi^2 d\varphi \\ &= 1 - \frac{1}{2\alpha} \int_0^{2\alpha} \left(1 - \frac{\varphi}{2\alpha} \right) \varphi^2 d\varphi = 1 - \frac{1}{2\alpha} \left(\frac{1}{3} \varphi^3 \Big|_0^{2\alpha} - \frac{1}{8\alpha} \varphi^4 \Big|_0^{2\alpha} \right) \\ &= 1 - \frac{1}{2\alpha} \left(\frac{8}{3} \alpha^3 - 2\alpha^3 \right) = 1 - \frac{1}{3} \alpha^2 \end{aligned} \quad (\text{A.7})$$

For the parallel orientation, the phase distribution as a result of the convolution of the trapezoidal with the rectangular shapes is piecewise quadratic and is defined according to

$$\rho_{\text{par}}(\varphi) = \frac{1}{32\alpha^3} \begin{cases} (\varphi + 4\alpha)^2 & \text{for } -4\alpha \leq \varphi < -2\alpha \\ (8\alpha^2 - \varphi^2) & \text{for } -2\alpha \leq \varphi \leq +2\alpha \\ (\varphi - 4\alpha)^2 & \text{for } +2\alpha < \varphi \leq +4\alpha \\ 0 & \text{else} \end{cases} \quad (\text{A.8})$$

This yields

$$\begin{aligned} M_{\text{par}} &= 1 - \frac{1}{2} \int_{-4\alpha}^{+4\alpha} \rho_{\text{par}}(\varphi) \varphi^2 d\varphi = 1 - \int_0^{4\alpha} \rho_{\text{par}}(\varphi) \varphi^2 d\varphi \\ &= 1 - \frac{1}{32\alpha^3} \left(\int_0^{2\alpha} (8\alpha^2 - \varphi^2) \varphi^2 d\varphi + \int_{2\alpha}^{4\alpha} (\varphi - 4\alpha)^2 \varphi^2 d\varphi \right) \\ &= 1 - \frac{1}{32\alpha^3} \left(\frac{8\alpha^2}{3} \varphi^3 \Big|_0^{2\alpha} - \frac{1}{5} \varphi^5 \Big|_0^{2\alpha} + \frac{1}{5} \varphi^5 \Big|_{2\alpha}^{4\alpha} - \frac{8\alpha}{4} \varphi^4 \Big|_{2\alpha}^{4\alpha} + \frac{16\alpha^2}{3} \varphi^3 \Big|_{2\alpha}^{4\alpha} \right) \\ &= 1 - \frac{1}{32\alpha^3} \alpha^5 \left(\frac{64}{3} - \frac{32}{5} + \frac{1024}{5} - \frac{32}{5} - 512 + 32 + \frac{1024}{3} - \frac{128}{3} \right) \\ &= 1 - \alpha^2 \end{aligned} \quad (\text{A.9})$$

i.e. a three-fold signal decay compared to the antiparallel orientation.

The signal for the parallel orientation can also be estimated less tediously by considering the two local phase distributions. The rectangular distribution for the parallel orientation, can be decomposed into a lower rectangle of half height and two triangles (Fig. A1). Shifting these triangles by $\pm 2\alpha$ yields the trapezoidal distribution of the parallel orientation. In other words, the two local phase distributions differ only by a shift of the two triangular contributions.

The signal decay according to Eq. (A.6) represents the second moment of $\rho(\varphi)$. Keeping in mind the parallel axes rule for the moment of inertia, it can be concluded that the second order term of the signal decay for $\rho(\varphi)$ shifted by φ_0 from its mean value, increases by $\varphi_0^2/2$, where the factor of 1/2 is the prefactor appearing in Eq. (A.6). The mean phases φ_0 of the triangles in Fig. A1 are $\pm\alpha/3$ for the antiparallel orientation and $\pm 5\alpha/3$ for the parallel orientation. Thus, the difference of the shift contributions to the signal decay for each triangle is given by $\frac{1}{2} \left[\left(\frac{5\alpha}{3} \right)^2 - \left(\frac{\alpha}{3} \right)^2 \right] = \frac{4\alpha^2}{3}$. Taking the

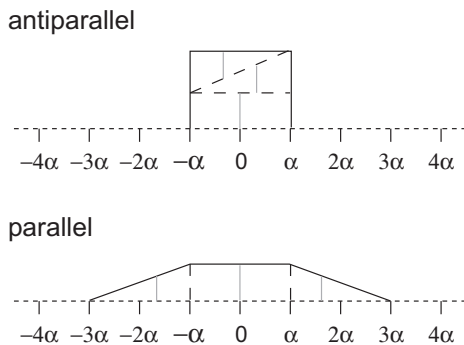


Fig. A1. Comparison of the final local phase distributions for antiparallel and parallel wave vector orientations. They are equivalent if the triangles are shifted accordingly. The gray lines indicate the mean phase for each sub-distribution. For details see text.

relative population of a triangle into account ($1/4$), the shift effect for each triangle is $\alpha^2/3$.

This value is identical to the antiparallel signal decay. Because the difference between the parallel and antiparallel signal decays was given only by the shift of the two triangular contributions, the signal decay of the parallel orientations is three times that of the antiparallel orientation. These considerations were based on the local phase distributions. However, as the total phase distribution effectively is the sum of the local distributions, the conclusion also holds for the sample's signal.

References

- [1] D.G. Cory, A.N. Garroway, J.B. Miller, Applications of spin transport as a probe of local geometry, *Polym Preprints* 31 (1990) 149–150.
- [2] P.T. Callaghan, B. Manz, Velocity exchange spectroscopy, *J. Magn. Reson. A* 106 (1994) 260–265.
- [3] P.P. Mitra, Multiple wave-vector extensions of the NMR pulsed-field-gradient spin-echo diffusion measurement, *Phys. Rev. B* 51 (1995) 15074–15078.
- [4] Y. Cheng, D.G. Cory, Multiple scattering by NMR, *J. Am. Chem. Soc.* 121 (1999) 7935–7936.
- [5] M.A. Koch, J. Finsterbusch, Compartment size estimation with double wave vector diffusion-weighted imaging, *Magn. Reson. Med.* 60 (2008) 90–101.
- [6] T. Weber, C.H. Ziener, T. Kampf, V. Herold, W.R. Bauer, P.M. Jakob, Measurement of apparent cell radii using a multiple wave vector diffusion experiment, *Magn. Reson. Med.* 61 (2009) 1001–1006.
- [7] N. Shemesh, E. Özarslan, P.J. Basser, Y. Cohen, Measuring small compartmental dimensions with low- q angular double-PGSE NMR: The effect of experimental parameters on signal decay, *J. Magn. Reson.* 198 (2009) 15–23.
- [8] M.E. Komlosh, E. Özarslan, M.J. Lizak, F. Horkay, P.J. Basser, Fiber diameter mapping of a white matter phantom using d-PFG filtered MRI, in: *Proceedings of International Society for Magnetic Resonance in Medicine, 18th Annual Meeting, Stockholm, Sweden, 2010*, p. 3393.
- [9] M.A. Koch, J. Finsterbusch, Double wave vector diffusion weighting in the human corticospinal tract in vivo, in: *Proceedings of International Society for Magnetic Resonance in Medicine, 16th Annual Meeting, Toronto, Canada, Germany, 2008*, p. 764.
- [10] M.A. Koch, J. Finsterbusch, In vivo pore size estimation in white matter with double wave vector diffusion weighting, in: *Proceedings of International Society for Magnetic Resonance in Medicine, 18th Annual Meeting, Stockholm, Sweden, 2010*, p. 194.